VICTORIA UNIVERSITY
MELBOURNE AUSTRALIA

Misfolded polyglutamine, polyalanine, and superoxide dismutase 1 aggregate via distinct pathways in the cell

This is the Published version of the following publication

The publisher's official version can be found at
https://www.sciencedirect.com/science/article/pii/S0021925820444849?via%3Dihub
Note that access to this version may require subscription.

Misfolded Polyglutamine, Polyalanine, and Superoxide Dismutase 1 Aggregate via Distinct Pathways in the Cell*[S]

Saskia Polling[‡], Yee-Foong Mok[‡], Yasmin M. Ramdzan[‡], Bradley J. Turner[§], Justin J. Yerbury[¶], Andrew F. Hill[‡], and Danny M. Hatters[‡1]

From the [‡]Department of Biochemistry and Molecular Biology and Bio21 Molecular Science and Biotechnology Institute, and [§]Florey Institute of Neuroscience and Mental Health and Centre for Neuroscience, The University of Melbourne, Victoria 3010, Australia, and the [¶]School of Biological Sciences, Faculty of Science and Illawarra Health and Medical Institute, University of Wollongong, Wollongong, New South Wales 2522, Australia

Background: Protein aggregation is associated with neurodegenerative diseases.
Results: We defined how the oligomeric state of disease-relevant mutant protein and homopolypeptides relate to clustering into inclusion subtypes IPOD and JUNQ.
Conclusion: JUNQ protein and homopolypeptides relate to constitutively disrupted oligomeric states irrespective of inclusion formation.
Significance: JUNQ inclusions may arise by cellular failure in degradation of abnormal oligomeric states.

Protein aggregation into intracellular inclusions is a key feature of many neurodegenerative disorders. A common theme has emerged that inappropriate self-aggregation of misfolded or mutant polypeptide sequences is detrimental to cell health. Yet protein quality control mechanisms may also deliberately cluster them together into distinct inclusion subtypes, including the insoluble protein deposit (IPOD) and the juxtanuclear quality control (JUNQ). Here we investigated how the intrinsic oligomeric state of three model systems of disease-relevant mutant protein and peptide sequences relates to the IPOD and JUNQ patterns of aggregation using sedimentation velocity analysis. Two of the models (polyalanine (37A) and superoxide dismutase 1 (SOD1) mutants A4V and G85R) accumulated into the same JUNQ-like inclusion whereas the other, polyglutamine (72Q), formed spatially distinct IPOD-like inclusions. Using flow cytometry pulse shape analysis (PulSA) to separate cells with inclusions from those without revealed the SOD1 mutants and 37A to have abruptly altered oligomeric states with respect to the nonaggregating forms, regardless of whether cells had inclusions or not, whereas 72Q was almost exclusively monomeric until inclusions formed. We propose that mutations leading to JUNQ inclusions induce a constitutively "misfolded" state exposing hydrophobic side chains that attract and ultimately overextend protein quality capacity, which leads to aggregation into JUNQ inclusions. Poly(Q) is not misfolded in this same sense due to universal polar side chains, but is highly prone to forming amyloid fibrils that we propose invoke a different engagement mechanism with quality control.

Protein aggregation underpins more than 35 human diseases including Huntington, Alzheimer, and motor neuron disease (1). A common theme in these diseases is that the formation of abnormal aggregates leads to a gain of toxic function to cells. Although we now have a reasonably detailed understanding of the mechanisms for how proteins misfold and assemble into amyloid-like structures *in vitro*, there is comparatively far less knowledge of the aggregation patterns in the cellular environment and how these patterns engage with, or are altered by the cellular machinery (2). This goal is important because emerging evidence indicates that cells employ protein quality control mechanisms to dictate the patterns of aggregates that form. These include chaperones that "disaggregate" and suppress aggregation, or at the other end of the spectrum mechanisms that deliberately sort misfolded proteins into protective clusters for sequestration and degradation (3–6). The active clustering of misfolded proteins can manifest as two or possibly more distinct inclusion subtypes (7, 8). The original compartment was defined as the aggresome, which described the microtubule-dependent sequestration of misfolded cystic fibrosis transmembrane conductance regulator (CFTR) protein to the microtubule organizing center for sequestration (8). More recent studies have refined the aggresome model into two subtypes: the juxtanuclear quality control (JUNQ)[2] and the insoluble protein deposit (IPOD) (7). JUNQ was described as a ubiquitin-proteasome-rich compartment for refolding recoverably misfolded proteins and the IPOD a sink for irreversibly aggregated proteins (7).

Collectively the overlapping processes of clustering proteins by protein quality control and the inherent aggregation propensities of misfolded proteins are blurred when examined by typical morphological assays. Hence our capacity to define what an

---

[S] This article contains supplemental Table 1.

[1] To whom correspondence should be addressed: Dept. of Biochemistry and Molecular Biology, Bio21 Molecular Science and Biotechnology Institute, 30 Flemington Rd., the University of Melbourne, Melbourne, VIC 3010, Australia. Tel.: 61-3-8344-2530; Fax: 61-3-9348-1421; E-mail: dhatters@unimelb.edu.au.

[2] The abbreviations used are: JUNQ, juxtanuclear quality control; EGFP, enhanced GFP; Httex1, huntingtin exon 1; i, inclusion; IPOD, insoluble protein deposit; ni, non-inclusion; poly(A), polyalanine; poly(Q), polyglutamine; PulSA, pulse shape analysis; SOD1, superoxide dismutase; SVA, sedimentation velocity analysis.

aggregate actually is in the cell, and more specifically the differences between the intrinsically self-aggregated forms of the proteins and actively formed clusters controlled by quality control processes remain limited (2).

Previously we developed several strategies to quantitatively map the patterns of aggregation of the huntingtin exon 1 fragment (Httex1) in the cell, which when mutated to contain an expanded polyglutamine (poly(Q)) sequence beyond an aggregation threshold of about 36 glutamines, forms dense inclusion bodies in neurons of Huntington disease tissues (9–12). SVA is a benchmark method for investigating mass heterogeneity of purified proteins (13), but to date has had limited application in cell lysates using fluorescently tagged proteins. We applied this method successfully to cell lysates to decipher the aggregation patterns of Httex1 and other proteins (10, 12, 14). We have also developed a strategy to separate cells expressing mutant protein enriched in inclusions from those lacking inclusions using Pulse Shape Analysis (PulSA) by flow cytometry, which enables a second layer of control over the study of protein oligomerization in cells with visible inclusions or not (11). PulSA is based on the principle that the fluorescence width and height parameters of a target protein in a cell vary with its cellular localization. We previously showed that PulSA can efficiently distinguish cells with a GFP-tagged protein localized diffusely throughout the cytoplasm from cells with a restricted spatial localization such as an inclusion. In particular, we showed we could separate mutants of superoxide dismutase 1 (SOD1) and Httex1 that had shifted from a dispersed unaggregated state to inclusions (11).

In this study, we combined SVA with PulSA to decipher how the oligomeric size distribution of three disease-associated proteins/modules, polyglutamine (poly(Q)), polyalanine (poly(A)), and SOD1 change in cells with a dispersed misfolded protein localization and cells with inclusions of different macroscopic properties. Aggregation-prone poly(A), poly(Q), and SOD1 mutants each form JUNQ- or IPOD-type inclusions, suggesting fundamental differences in how the quality control system engages with the mutant proteins and homopolypeptide sequences (15–17). When mutated to lengths beyond a threshold of approximately 37 glutamines, poly(Q) leads to aggregation in nine different proteins and corresponding human diseases (18). The capacity to aggregate into inclusions is encoded strictly within the extended poly(Q) (19, 20). Likewise, mutations that expand poly(A) lengths to beyond a threshold of approximately 18 alanines lead to disease in nine different proteins (21). The poly(A) sequences crossing this disease-length threshold also lead to clustering into inclusions (22, 23). Mutations in SOD1 that lead to amyotrophic lateral sclerosis are also associated with the formation of inclusions (24).

EXPERIMENTAL PROCEDURES

Plasmids—The pEGFP-N1 vectors containing human SOD1[WT], SOD1[A4V], SOD1[G85R], and SOD1[G93A] were generated as described (25). The pEGFP-C1 vectors containing polyalanine repeats of 7 alanines or 37 alanines were generated as described (22) and the mCherry versions made by swapping out EGFP using standard cloning procedures. Amino acid sequences of the translated proteins are shown in supplemental Table 1.

EGFP-LC3 was generated as described (26). Httex1 vectors and poly(Q) vectors were produced as described (9).

Cell Culture—Human Embryonic Kidney Adherent (AD293) cells were maintained in Dulbecco's modified Eagle's medium (DMEM) supplemented with 1 mM glutamine, 200 units/ml penicillin/streptomycin, and 10% v/v fetal bovine serum. Cells were kept at 37 °C in a humidified incubator with 5% atmospheric CO_2. For confocal microscopy cells were plated on poly-L-lysine-coated 8-well μ-slide (Ibidi), whereas for SVA and flow cytometry sorting, cells were plated on 75-cm² tissue culture flasks. Cells were transfected using Lipofectamine 2000 according to the manufacturer's instructions with 0.5 μg of DNA and 24 μg of DNA for the μ-slides and 75-cm² flasks, respectively, and a DNA:Lipofectamine ratio of 1:2.5 w/v (Invitrogen). Medium was refreshed 6 h after transfection.

SVA—Cells grown on 75-cm² flasks were harvested in phosphate-buffered saline (PBS) 72 h after transfection with a cell scraper. For cells collected by flow cytometry, $\sim 2 \times 10^5$ cells were collected for each population (*i.e.* ni and i). Cells were pelleted ($180 \times g$, 6 min, room temperature) and snap-frozen in liquid nitrogen. Cell pellets were thawed on ice and lysed and prepared for SVA as described previously (10). In essence, the cell pellets were extruded 25 times through a 27-gauge needle in an ice-cold solution of 20 mM Tris, 2 mM $MgCl_2$, 150 mM NaCl, 1% w/v Triton X-100, pH 8.0, supplemented with EDTA-free protease inhibitor mixture (Roche Applied Science) and 20 units/ml Benzonase. Total protein levels in the cell lysate were measured using a bicinchoninic acid assay with bovine serum albumin as the mass standard. Single-use aliquots were snap-frozen in liquid nitrogen and stored at −80 °C. Crude fluorescence levels of 100 μg of total lysate protein were assessed in a plate reader and adjusted, where necessary, to similar levels by dilution into untransfected cell lysate to maintain a similar cellular protein concentration and target EGFP-tagged protein concentration. Samples were assessed by SVA at 10 °C as previously described using a total cellular protein concentration of 0.5 mg/ml. In essence, samples were adjusted to 0 or 2 M sucrose by addition of freshly prepared 3 M sucrose, added by weight. Sucrose stock solutions were made by heating sucrose with water and calibrated for concentration by refractive index at 20 °C (27). Final sample sucrose concentrations were re-verified by refractive index. Samples were loaded into two-channel Quartz window sedimentation velocity cells (Beckman-Coulter) with 50 μl of FC-43 heavy oil (Fluorinert). Cells were placed in a prechilled 8-hole AnTi rotor (Beckman-Coulter) and equilibrated to 10 °C in an XL-A analytical ultracentrifuge (Beckman-Coulter) fitted with a fluorescence detection system (Aviv). Radial fluorescence scans were collected continuously at 50,000 or 3,000 rpm using a 488-nm laser for excitation and 520-nm cut-off emission filter and with the photomultiplier voltage kept constant in each experiment. Data were fitted to c(s) distributions as described (10, 28).

Flow Cytometry and Sorting—Cells were analyzed by PulSA as described (11). For sorting experiments, 2×10^7 transfected cells were detached through scraping in 1 ml of PBS supplemented with 10 units/ml DNase I, 5 mM $MgCl_2$, and 0.1% w/v bovine serum albumin (BSA). Flow cytometry grade tubes were precoated for 30 min with 0.5% w/v BSA. Prior to sorting cells

were filtered through a nylon mesh. Cells were sorted on a FAC-SAria cell sorter using a 70-μm nozzle and on data collected for pulse height, width, and area of EGFP with a FITC (530/30) filter. Side scatter and forward scatter height and width were also collected. For analysis, cells were gated to remove debris and doublet cells using the forward scatter (FSC-A) and side scatter (SSC-A) plots as described (11). Cells were kept on ice for all steps of the sorting preparation and handling. FlowJo was used for graphical representation and analysis.

Confocal Microscopy—Cells were fixed 26 h after transfection in 4% w/v paraformaldehyde for 10 min at room temperature. For immunostaining (except γ-tubulin) cells were incubated in 50 mM NH$_4$Cl for 10 min, followed by permeabilization in 0.1% v/v Triton X-100 for 4 min at room temperature. For γ-tubulin staining, cells were instead fixed and permeabilized with methanol (10 min at -20 °C). Samples were blocked in 1% w/v BSA for 20 min at room temperature. Primary antibodies and dilutions used were rabbit anti-proteasome-20S-C2, 1:500 (Ab3325; Abcam); mouse anti-vimentin, 1:50 (MAB3400; Millipore); mouse anti-γ-tubulin GTU88, 1:500 (Sigma); mouse anti-ubiquitin (FK2), 1:250 (Millipore). Cells were washed in PBS for 30 min. Samples were incubated with Alexa Fluor 488, Alexa Fluor 643, or Cy3-conjugated secondary antibody for 30 min at room temperature (Invitrogen). Cell nuclei were stained with 6.5 μM Hoechst 33342 for 15 min at 37 °C. Cells were rinsed in PBS between all steps. To apply confocal microscopy on FACS-sorted cells, sorted cell suspensions were incubated with a final concentration of 2% w/v paraformaldehyde for 20 min at room temperature. After fixation cells were pelleted at 180 × g for 6 min. Pellets were subsequently resuspended in 5 μl of PBS and spotted onto a no. 1.5 glass microscopy slide. To limit volume dispersion a barrier was applied onto the slide using a liquid blocking PAP pen. Slides were sealed using a glass coverslip and nail polish. Cells were imaged immediately after using a 40× NA 1.25 or 100× NA 1.4 oil objective on a Leica SP2 or SP5 inverted confocal microscope. ImageJ and Adobe illustrator CS5 were used for image processing.

RESULTS

To establish the IPOD and JUNQ patterns of localization of our model protein/homopolypeptide systems, we first expressed EGFP or mCherry-tagged mutant (aggregating) and nonmutant (nonaggregating) forms of our proteins individually and together in pairs in AD293 cells (sequences of constructs in supplemental Table 1). Our objective was to evaluate the morphological and co-localization patterns of inclusions that arise. Essentially the nonmutant proteins, poly(A) (with 7A), poly(Q) (with 25Q), Httex1 (with 25Q), and SOD1 (wild type) never formed inclusions and were evenly distributed throughout the cytosol, as has been well established previously (9, 22, 25 and data not shown).

The A4V and G85R mutants of SOD1, both of which lead to a familial form of amyotrophic lateral sclerosis, have previously been reported to form inclusions (25, 29, 30). Inclusions formed by these proteins had an apparent porous, labyrinthine topology in a small proportion of the cells (~10% of the transfected population) (Fig. 1), with most cells otherwise retaining an evenly diffuse pattern similar to the wild-type SOD1 (data not

shown). Co-expression of both SOD1 mutants together, using different EGFP and mCherry tags to distinguish them, revealed that of the cells containing inclusions of both mutants, in all cases the inclusions were completely overlapped in spatial localization of the EGFP- and mCherry-tagged proteins (Fig. 1). For poly(A)-mCherry containing an aggregation-prone alanine length (37A) inclusions were observed in ~10% of the transfected cells that appeared similar in morphology to the SOD1 inclusions. These inclusions also overlapped completely in spatial localization when 37A-mCherry was co-expressed with both EGFP-tagged SOD1 mutants for all cells where both proteins aggregated (Fig. 1). In transfected cells lacking inclusions the protein was otherwise diffusely distributed throughout the cytosol in a manner similar to 7A (data not shown). Collectively these observations show that when 37A and the two SOD1 mutants aggregate in the same cell they coalesce into a common inclusion structure.

Two polyglutamine-containing proteins, either in context of the Huntington exon 1 (46Q) fused to mCherry, or with appending huntingtin sequence removed (72Q) and fused to EGFP, aggregates appeared in ~30% of the transfected cells whereas in cells lacking inclusions, the proteins were evenly dispersed throughout the cytosol, patterns of localization which have been well established elsewhere (data not shown and Refs. 31, 32). For the cells with aggregates, the aggregates exhibited a dense punctate pattern unlike that observed for the 37A and SOD1 mutants. Co-expression of Httex1(46Q)-mCherry with EGFP-72Q revealed that the two tagged proteins coalesced into completely overlapping patterns of localization in cells with inclusions (Fig. 1). However, when Httex1(46Q)-Cherry was co-expressed with the SOD1 mutants fused to EGFP (or 37A fused to EGFP), aggregates that formed in the same cell were always completely spatially excluded from each other, indicating that the inclusion structures of these two proteins are fundamentally distinct from each other (Fig. 1).

Prior work has indicated that poly(Q) can partition to an IPOD-like structure and that the SOD1 G93A mutant partitions to the JUNQ (16). Hence, our data confirmed the nominal classification of poly(Q)-containing proteins accruing into an IPOD-like inclusion, whereas poly(A) and SOD1 molecules accrue into a JUNQ-like inclusion. Both inclusions do not overlap spatially to any extent and hence form completely different structures in the cells.

To investigate these inclusion types in more detail we examined cellular protein markers previously reported to indicate similarities and differences for the aggresome, IPOD and JUNQ inclusions (Fig. 2). In all cells with inclusions, we observed a restructuring of vimentin intermediate filaments, a feature of inclusion formation reported originally for the aggresome model, which was absent in cells lacking inclusions (Fig. 2A) (8). All inclusion types were proximal to the γ-tubulin puncta, which is also consistent with previous observations related to positioning of inclusions near the microtubule organizing center (Fig. 2B, *arrows* mark microtubule organizing center) (8). The SOD1 and poly(A) inclusions showed little or no co-localization with EGFP-LC3, a marker of autophagic vesicles, whereas there was partial enrichment of LC3 around the 72Q inclusions (Fig. 2C). The SOD1 and poly(A) inclusions showed
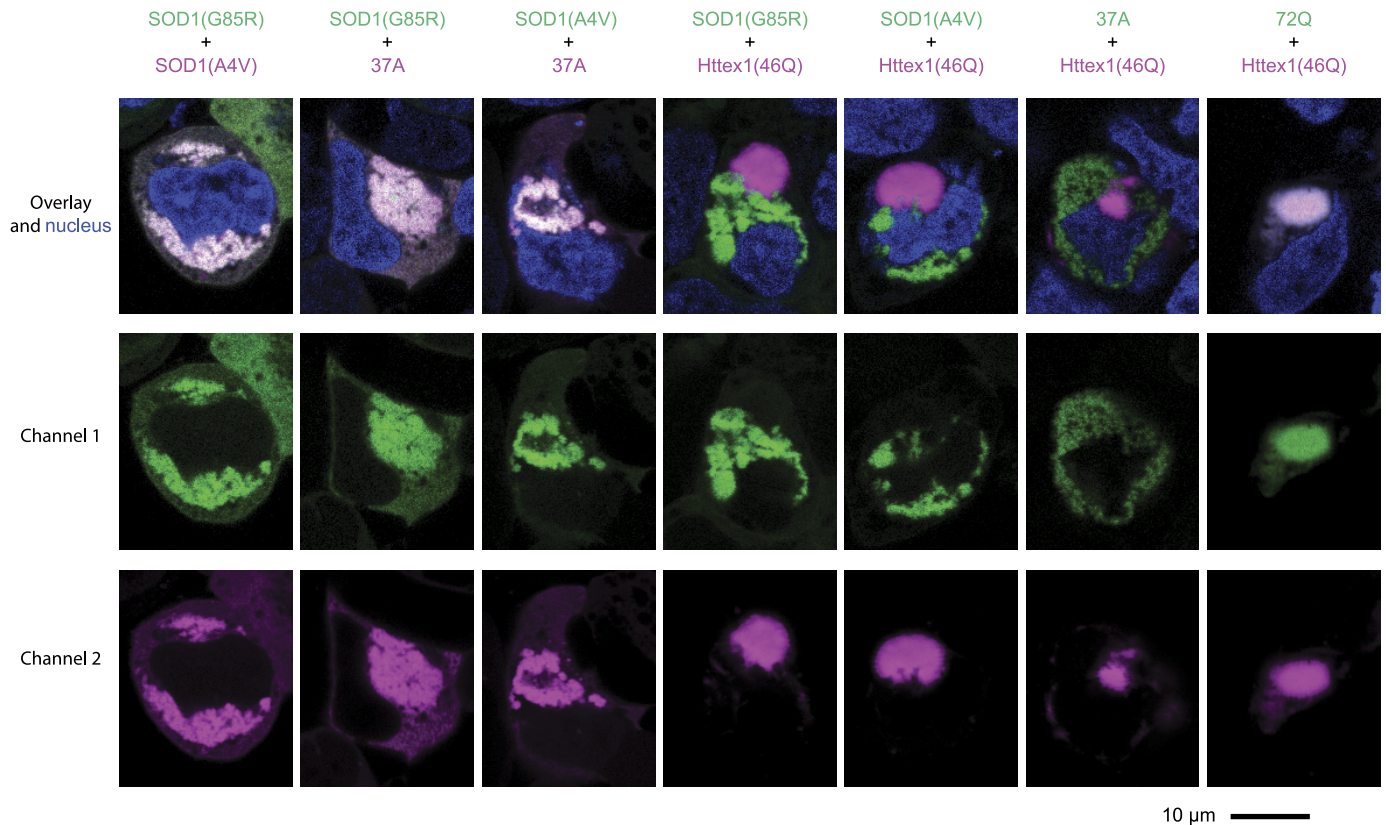
FIGURE 1. **Aggregation-prone SOD1, poly(Q), and poly(A) partition into two distinct inclusion patterns.** Data show co-transfections in AD293 cells after 26-h expression. *Green* shows EGFP-tagged constructs, *magenta* shows mCherry-tagged constructs, and *blue* shows a nuclear stain (Hoechst 33342). The nonaggregating counterparts did not form inclusion structures either alone or co-transfected with any combination of nonaggregating or aggregating protein.

pronounced co-localization with ubiquitin (Fig. 2D) and proteasomes (Fig. 2E), whereas there was no noticeable enrichment with the 72Q inclusions. These results are consistent with the SOD1 and poly(A) inclusions being more actively engaged with proteasome-mediated degradation processes than the poly(Q) inclusions, which may instead be engaged more extensively with autophagy-mediated degradation. These results show a divergence in quality control engagement with these inclusion types and show patterns of localization of markers that are nominally consistent with the JUNQ and IPOD models for sorting of misfolded proteins (7).

We next employed our SVA method to assess the oligomeric state of the three different mutant and nonmutant proteins (SOD1-EGFP, EGFP-poly(A), and EGFP-poly(Q)). We adopted our previously devised procedure which visualized all oligomeric forms of Httex1(46Q)-EGFP in cell lysate by running samples in parallel format under three different conditions (10). First we performed high speed spins (50,000 rpm) which are designed to capture the sedimentation profiles of soluble, low oligomeric forms of proteins in the lysate, with the caveat that high mass material completely pellets before data can be acquired. To capture the profile of larger mass material, we performed low speed spins (3,000 rpm). Finally to capture any remaining material evading detection under the low speed spin, we performed low speed spins with the lysate supplemented with 2 M sucrose to increase viscosity, enabling massively aggregated protein to be captured in the sedimentation profile.

Initial assessments of the cell lysates for EGFP fluorescence intensity revealed that the mutant proteins yielded far lower levels of protein than the nonaggregating counterparts, which is suggestive of greater rates of degradation (Fig. 3A). Whereas the lower levels of protein can be partly explained by slightly reduced transfection rates of the mutant proteins (Fig. 3B), it also remains plausible that the mutant proteins are degraded more effectively than the wild-type forms based on the data in Fig. 2 showing enrichment of degradation machinery (*i.e.* ubiquitin, proteasomes, and/or LC3) with the JUNQ and IPOD inclusions. Using PulSA, we estimated the proportion of transfected cells with inclusions to be 50% for EGFP-72Q, 15% for EGFP-37A and 5% for the SOD1(A4V)-EGFP, similar to our estimates for the data in Fig. 1 (note that the cells for this experiment were cultured and transfected under conditions different from those in Fig. 1 which can affect rates and extents of aggregation).

To account for possible protein concentration differences influencing steady-state oligomeric state during SVA, we standardized GFP fluorescence intensities of the lysates for each set of mutants by adding untransfected lysate prior to SVA. The time series of sedimentation profiles of the lysates are shown in Fig. 4, *A–C*. For the high speed scans the entire fluorescent signal of each protein formed an incrementing series of sedimenting boundaries (Fig. 4A). These data were fitted to a size distribution model, $c(s)$, to yield the molecular size heterogeneity of the target GFP-tagged proteins in the lysate. As a control,
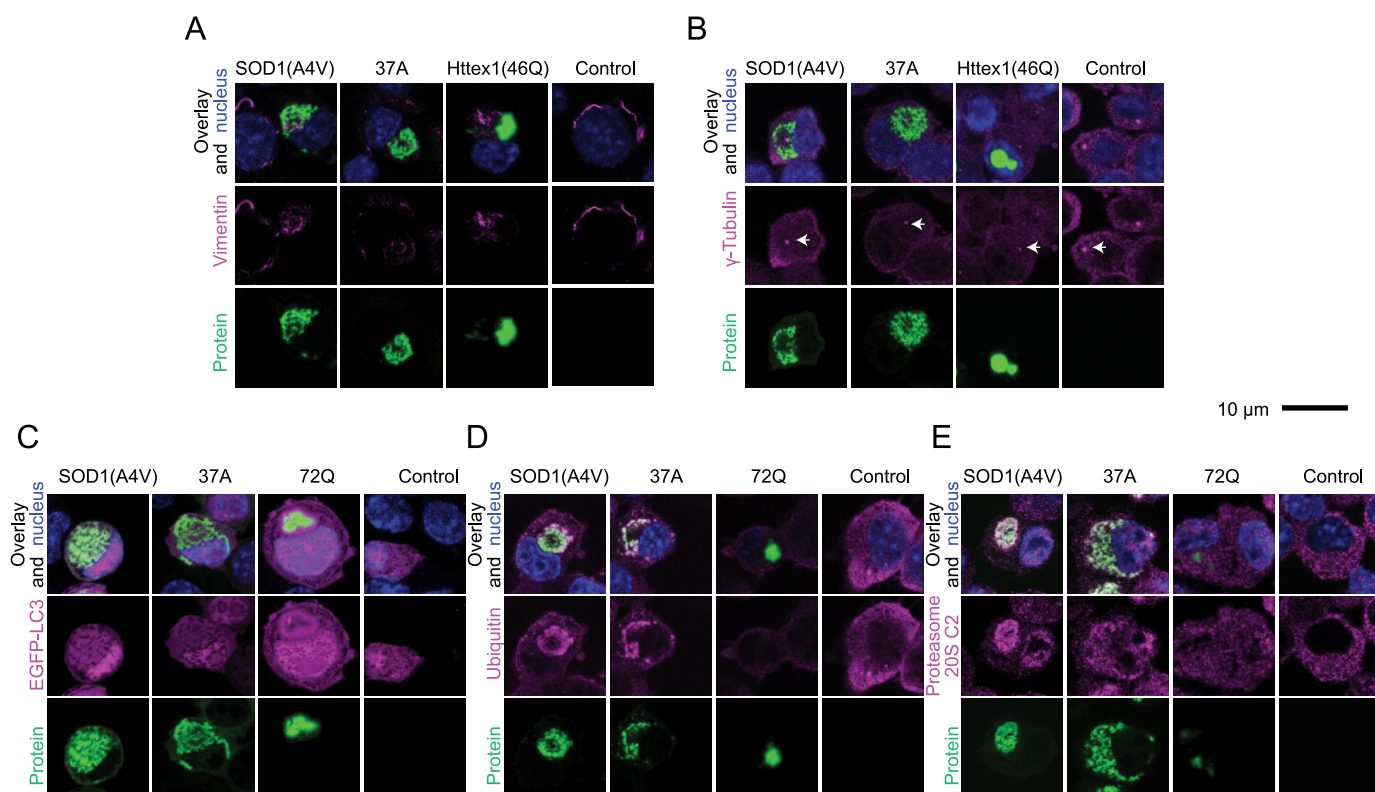
FIGURE 2. **Patterns of cellular markers for the two distinct inclusion types.** Cells were transfected with Emerald-, EGFP-, or mCherry-tagged mutant proteins/homopolypeptides for visual detection or with GFP immunofluorescence for methanol-fixed samples. Endogenous vimentin (*A*), γ-tubulin (*B*), ubiquitin (*C*), and proteasome subunit 20S C2 (*E*) were detected by immunofluorescence. EGFP-LC3 (*D*) was co-transfected with the mutant protein. Control cells were transfected with a nonfluorescent Y66L GFP derivative, as described previously (10). Images are *colored coded* as shown, with *blue* indicating a nuclear stain (Hoechst 33342).

EGFP alone sedimented as a single species consistent with monomer as reported previously (10, 14) (Fig. 5*A*). EGFP-poly(Q) in both nonmutant (25Q) and mutant (72Q) forms was also entirely monomeric under these conditions (Fig. 5*A*). EGFP-poly(A), however, revealed a distinct sedimentation pattern. Nonmutant (7A) was entirely monomeric, whereas the mutant (37A) formed a mixture of monomers and small oligomers spanning sedimentation coefficients of 7–20 S, which corresponds to oligomers of ≈4–20 units assuming no interactions with additional cellular ligands (Fig. 5*A*). Wild-type SOD1-GFP was predominantly dimeric whereas the A4V mutant was almost entirely monomeric (Fig. 5*A*). The G85R mutant also revealed a greater abundance of monomers, suggesting that mutations in SOD1 that lead to JUNQ formation abruptly destabilize the native dimer state (Fig. 5*A*). These results demonstrated that low mass forms of EGFP-poly(Q) remained primarily monomeric regardless of poly(Q)-length, whereas the JUNQ-forming proteins both had abruptly altered oligomeric state albeit in different ways.

Analysis of the low speed run, which captures larger sized oligomers, showed a flat unchanging boundary in the time series for all mutant proteins, indicating an absence of aggregate masses in this intermediate size range (∼100–3000 S) (Fig. 4*B*). For the low speed run in 2 M sucrose, which captures massively aggregated proteins such as inclusion-localized protein, the raw time series scans of the poly(Q) mutant showed a major proportion of the poly(Q) molecules sedimented, characteristic of the inclusion-localized protein of very large mass (Fig. 4*C*).

The apparent noise in the data is similar to what we previously observed for Httex1(46Q) inclusions and which we attributed to the inclusions being large enough individually to move in and out of the laser beam focal point during the scans (10), which precludes the ability to fit the data unequivocally. However, we estimated the sedimentation coefficient to be in the order of 100,000–1,000,000 S, similar to what we previously measured for Httex1(46Q) inclusions (mode $s_{20,w}$ of 320,000 S (10)). We observed a small level of the "noise" for 37A and mutant SOD1 proteins in early scans, but the proportion of signal was too small to discern as a clear sedimenting boundary. This suggested that 37A and SOD1 mutants had a small quantity of high mass material but that it represented <5% of the total SOD1-EGFP molecules in the cell lysate. This is broadly consistent with the data in Fig. 3, suggesting that no more than 10–15% of the cells transfected with SOD1 mutants or 37A formed inclusions.

By summing the proportions of different masses of each of the three spin conditions, we could estimate the proportion of molecules partitioning into the different oligomer categories (Fig. 5*B*). In essence, poly(Q) shifted from predominantly monomer to massively aggregated inclusion forms in a highly cooperative manner, consistent with 50% of the cells in the population forming inclusions. 37A and SOD1 mutants, however, shifted fundamentally in steady-state oligomeric status relative to the nonaggregating counterparts, despite the presence of inclusions in <10–15% of the cells, and massively aggregated forms in <5% of the total pool of molecules. These results
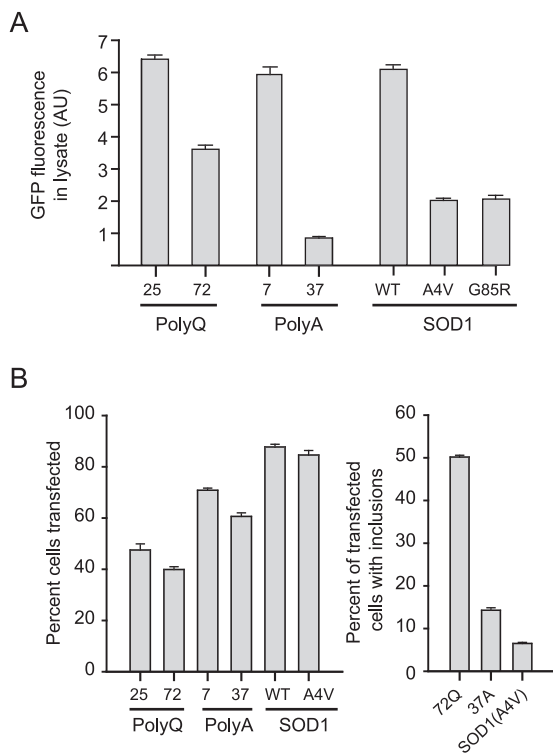
FIGURE 3. **Expression level and inclusion formation rates of AD293 cells transfected with model aggregating proteins and homopolypeptides.** *A*, cells were harvested after 72 h transfection and lysed in a nondenaturing Triton X-100-based buffer. Data show EGFP fluorescence standardized to 100 μg of total cellular protein ($n = 3$; mean $\pm$ S.D. (*error bars*) are shown). *B*, flow cytometry analysis was performed of cells harvested 72 h after transfection ($n = 3$; mean $\pm$ S.D. is shown). Data show transfection efficiency as standardized to a gate (FITC channel) defining 98% background fluorescence using untransfected cells as a reference. The percentage of transfected cells with inclusions was defined using PulSA as described previously (11, 12), with the nonaggregating mutants to set the reference gate positions ($n = 3$; mean $\pm$ S.D. are shown).

hence suggest that mutations that lead to JUNQ inclusions constitutively change the oligomeric state as a prelude to further aggregation into massively aggregated forms within the inclusions.

To probe more clearly the relationship between inclusion formation and oligomeric state, we applied PulSA with a sorting flow cytometer to separate and recover cells with inclusions from those without for further analysis by SVA. Fig. 6*A* shows the strategy of PulSA, which we used previously to track inclusion formation of Httex1 and SOD1 (11). In essence, gates can be defined based on pulse width and height parameters that match the localization patterns of GFP fluorescence in cells for dispersed protein (noninclusions, the ni gate) or condensed protein localizations (inclusions; the i gate) (Fig. 6*B*). Poly(Q) formed a far sharper contrast between the i and the ni populations than for the SOD1 and 37A mutants when using the nonaggregating counterparts to set the gate boundaries, reflecting poly(Q) inclusions being more condensed than the SOD1 and 37A inclusions (Fig. 6*B*). This was attributed to the SOD1 and 37A JUNQ labyrinthine morphology not providing a stark contrast in localization compared with cells with unaggregated proteins as was observed for the punctate 72Q inclusions and that protein levels were much lower in the mutant cell population than the wild-type counterpart, which also influences the

cytogram contour shapes. Nonetheless, the gating strategy led to a clear and robust enrichment of transfected cells with inclusions (>90% of cells) from cells without (<5% of cells with inclusions) for all mutants, as determined by visual inspection of the sorted populations by microscopy (Fig. 6*C*). The i- and ni-enriched populations of cells expressing 37A and SOD1 mutants were collected and assessed by SVA to determine the partitioning of the different oligomer and aggregate levels (Fig. 6, *D–F*). For 37A, the high speed spin revealed the presence of low mass forms in cells with inclusions as well as cells lacking inclusions (Figs. 6*D* and 7*A*). This likely reflects retention of a proportion of the diffuse cytoplasmic localized protein in the cells with the JUNQ inclusions. Of this soluble pool, there was no difference in proportion of monomer/small oligomers between the i- and ni-enriched populations, or notable differences in the size heterogeneity of the abnormal oligomers (Figs. 6*D* and 7, *A* and *C*). This result confirms that poly(A) expansions fundamentally alter the steady-state oligomerization and that this happens in a manner independently to presence of inclusions. This also suggests that aggregation of EGFP-37A into inclusions is not rate-limited by the formation of abnormal oligomers, because it could be expected that the oligomers would be rapidly sequestered into the inclusions in a nucleation-dependent model of aggregation. The low speed spin revealed no detectable levels of other larger oligomeric or aggregated forms (smaller than masses for inclusions) in cells with or without inclusions (Fig. 6*E*). This suggests that further aggregation intermediates to inclusion formation, such as amyloid-like "oligomers" or protofibrillar structures do not exist or are infrequently populated in cells (Fig. 6*E*). The low speed spin on lysate supplemented with 2 M sucrose revealed the i-enriched population to contain ~60% of the EGFP-37A molecules to be massively aggregated, confirming that the inclusions comprise largely of massively aggregated forms of these proteins and with the remainder solely of the monomer and abnormal oligomer (Figs. 6*F* and 7*C*).

The patterns observed for SOD1 mutants paralleled that observed for the poly(A) in terms of abundances of abnormal oligomeric state (*i.e.* monomers) and the massively aggregated masses. In essence, the A4V and G85R mutants both profoundly increased the proportion of monomer in the soluble pool of SOD1-EGFP relative to the dimer (Figs. 6*D* and 7*B*). This change in monomer:dimer ratio occurred to the same extent in cells with or without inclusions (Fig. 7, *B* and *C*). As with the EGFP-37A, the cells enriched for inclusions yielded a substantial proportion of massively aggregated masses, *i.e.* ~50% of the molecules were in massively aggregated forms (Figs. 6*F* and 7*C*). Again, as with EGFP-37A, there were no other intermediate sized oligomers or aggregates detected between the monomer/dimer states and the massively aggregated inclusion state (Figs. 6*E* and 7*C*). Collectively these data indicate the JUNQ-forming proteins of this study partition into a trimodal population: inclusions containing massively aggregated proteins, the normal oligomeric state seen with the wild-type counterparts, and an additional abnormal oligomeric state that is formed pervasively and independently from the massively aggregated state (Fig. 7*C*).
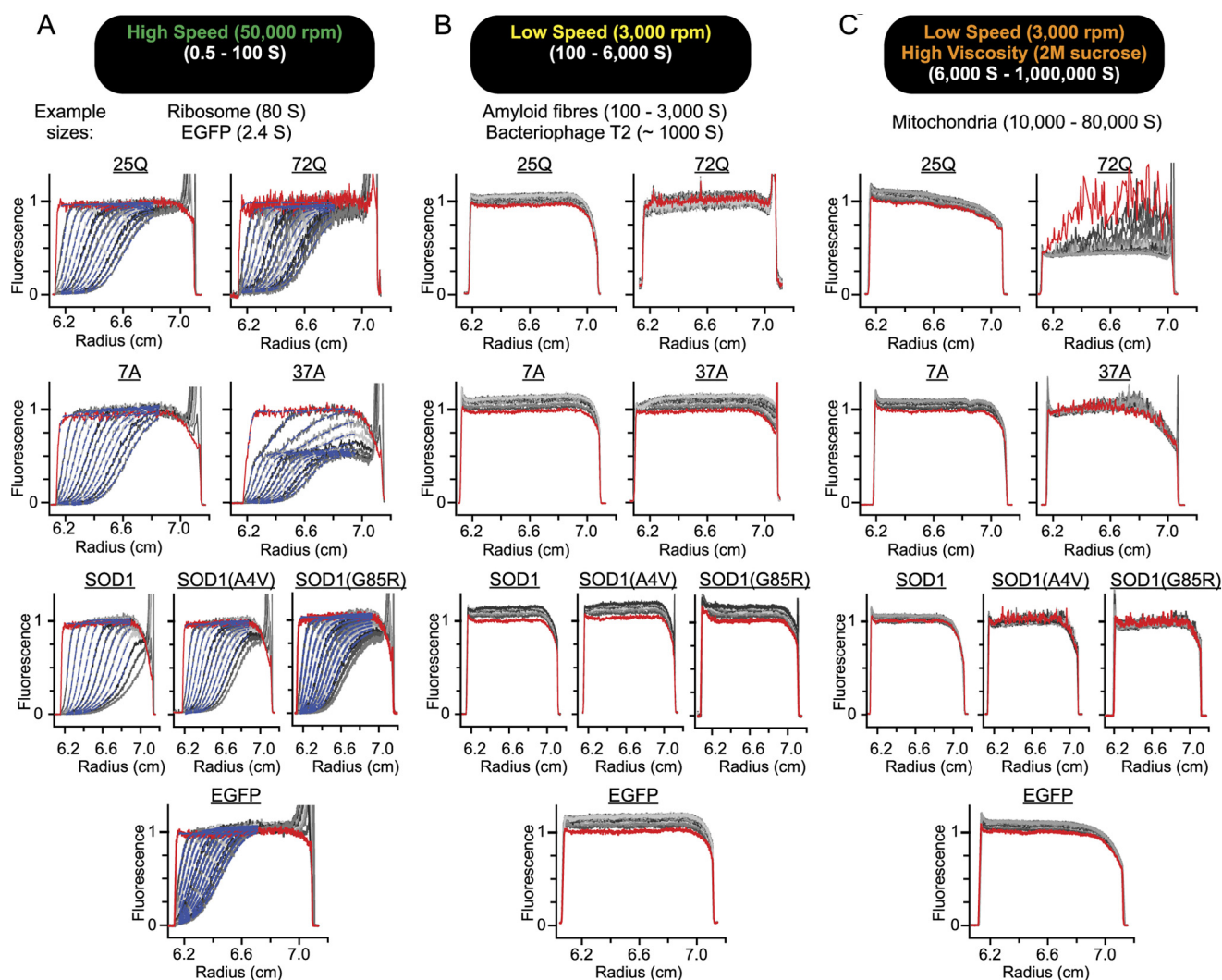
FIGURE 4. **SVA of EGFP-tagged proteins in crude AD293 cell lysate.** Cells were harvested after 72-h transfection with the EGFP-tagged proteins indicated on panels for SVA. Data show representative raw data set of one of three replicate experiments. Proteins were assessed at a total cell protein concentration of 0.5 mg/ml. Data show raw scans for the high speed analysis (*A*), parallel SVA at low speed (*B*), and parallel analysis of lysate supplemented with 2 M sucrose at low speed (*C*). Data show raw scans in *gray scale*, collected at incrementing timepoints upon centrifugation with the first scan shown in *red*. Data are normalized to the mid-point radius fluorescence intensity of the first scan. The *blue dashed lines* show fits of the raw data to a c(s) size distribution model (33).

DISCUSSION

We have described the changes in oligomeric state of three classes of disease-associated misfolded protein and homopolypeptide modules in cells that form different types of inclusion bodies. Of note was that the two classes that formed JUNQ-like structures, poly(A) and SOD1, were both fundamentally altered in steady-state oligomeric state relative to the nonaggregating counterparts whereas poly(Q), which formed an IPOD-like inclusion, remained mostly monomeric prior to inclusion formation. Hence the fundamental change at the steady-state oligomerization may dictate the inclusion type that forms. An explanation for this result is that mutations that change steady-state oligomerization arise through changes in exposure of hydrophobic stretches of amino acids, akin to the "misfolded state" of a globular soluble protein. Whereas amide backbone interactions can significantly contribute to the general stability of protein aggregates, especially amyloid fibrils (34), the hydrophobic side chains likely provide a more pivotal role in the mechanisms for SOD1 and 37A aggregation and JUNQ forma-

tion. Poly(A) is inherently hydrophobic; hence, extensions in poly(A) length beyond a critical threshold would enhance hydrophobicity to a level that enables small oligomers to form by the clustering together via the side chain methyl groups (possibly via clustered α-helices), as has been shown for *in vitro* studies on poly(A) peptides that assemble into globular micelle-like structures (35). Likewise, mutations in SOD1 that destabilize the dimer and ability to fold properly can lead to dissociation into misfolded monomers (36–38), which will disrupt the hydrophobic core of the protein. This may enable "exposure" of hydrophobic sequences and attraction of quality control mechanisms such as the hsp40·hsp70 chaperone systems (6). Whereas destabilization in globular structure may be necessary to open folding pathways permissive to fibril formation (24, 39, 40), it is possible that the prime aggregation problem in the cell arises not through misfolding down the amyloid fibril pathway but more acutely at the initial misfolded state, which likely prompts a robust response from quality control systems. It is notable that both SOD1 and poly(A) only form fibrils when
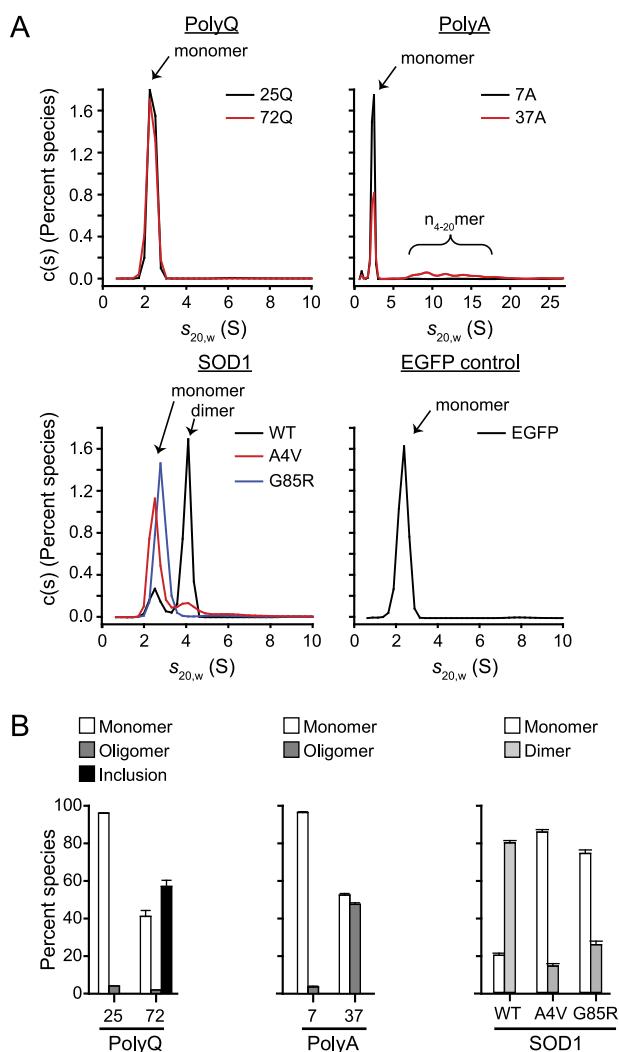
FIGURE 5. **Size distributions and molecular partitioning of EGFP-tagged protein and homopolypeptides in crude AD293 cell lysate.** *A*, *c*(*s*) size distributions of the fitted data from Fig. 4, with the estimated (homo)oligomeric state indicated. *B*, proportion of molecules in major oligomeric classes ($n = 3$; mean $\pm$ S.D. (*error bars*) are shown). For the small oligomers proportions were determined from area under curve as presented in Fig. 4*A*. For the inclusion masses, the proportions were determined from proportion of fluorescence intensity sedimenting as presented in Fig. 4*C*.

and JUNQ-like inclusions remains to be fully determined. Although there is evidence for active mechanisms driving the formation of the poly(Q)-type inclusions for benefit to cell survival (5), it remains plausible that the JUNQ-like structure represents spontaneous clustering of proteins exposing hydrophobic patches that have failed to be appropriately removed by the quality control system. Prior studies have suggested that the JUNQ operates to refold or degrade salvageable misfolded proteins and that proteins are diverted to the IPOD under conditions of irreversible aggregation (7). However, because we observed very few JUNQ-like inclusions (<10–15% of cells), it seems that the formation of inclusions of SOD1 is a secondary outcome to the fundamental change in steady-state oligomeric state. Furthermore, we never observed any evidence of co-aggregation of poly(A) or SOD1 into poly(Q) inclusions, suggesting that the JUNQ proteins are not converted into IPOD inclusions. Prior work has found that SOD1 inclusions correlate with poor cell survival relative to cells lacking inclusions suggesting that inclusions form under extreme duress at a near terminal state which seems mechanistically inconsistent with them acting as a precursor to the IPOD (37). We propose an alternative model for the SOD1- and poly(A)-type inclusions that arise through the loss of quality control capacity to prevent the abnormal steady-state oligomeric forms from aggregating. Misfolded soluble SOD1 can form complexes with chaperones hsp40 and hsp70, but the levels of soluble misfolded SOD1 eventually decline with age, suggesting that quality control systems can cope with processing the misfolded monomer for extended periods of time before failure at late stages of pathogenesis (48). It is also noteworthy that many of the diseases associated with poly(A) expansion mutations lead to decreased mutant protein levels under physiological expression levels, consistent with the quality control machinery efficiently recognizing the poly(A)-expanded mutant as misfolded and targeting them for degradation (21). This effect may be less pronounced for proteins that are naturally highly abundant, such as SOD1, mutants of which would demand a major constitutive commitment from the quality control network to cope with. By corollary this would confer far greater risk of collapse of global quality control systems upon further challenges to the protein quality control system. Because SOD1 is in the top 5% of abundance in most cell types (49), this mechanism provides an attractive hypothesis as to why so many mutants of SOD1 can cause amyotrophic lateral sclerosis if a common feature is to lead to improperly folded forms.

Another element to this model is that quality control resources are shared to some extent in the formation of IPOD and JUNQ-like inclusions. This has been shown by expression of temperature-sensitive proteins in *Caenorhabditis elegans* that are normally kept folded under permissive temperatures and which aggregate to form inclusions when pathogenic poly(Q) lengths are co-expressed (50). In these models, the poly(Q) inclusions formed distinct inclusion structures to the temperature-sensitive proteins, akin to the JUNQ and IPOD inclusions (50). A recent study suggested that poly(Q) inclusions sequester and trap hsp40 chaperone DNAJB1, which bxprevents it from delivering a misfolded carboxypeptidase Y proteins into the nucleus for degradation. A downstream con-

treated to harsh solution conditions or extreme temperatures *in vitro*, suggesting that fibrillization of these proteins may not be relevant to aggregation mechanisms that proceed in a cell (35, 41).

The mutations in this context differ markedly from the behavior of poly(Q). Poly(Q) is a more polar sequence and adopts a largely disordered and/or heterogeneous conformation in solution, indicating it to not be biophysically akin to a misfolded state of a globular protein (42). Poly(Q) readily assembles into amyloid-like fibrils stabilized by backbone-β-sheet interactions, which are also further stabilized by polar zipper interactions of the side chains (43–47). It is conceivable the lack of hydrophobic exposure of pure poly(Q) triggers a different engagement strategy from quality control to proteins that are misfolded, which ultimately leads to the IPOD.

The mechanisms by which the quality control system molds the clustering of the aggregates into the two different IPOD-

FIGURE 6. **SVA of EGFP-tagged protein and homopolypeptides in cells separated between those with and those without inclusions.** *A*, principle of PulSA by flow cytometry for defining cells with inclusions from cells lacking inclusions and its application to sort cells into inclusion (*i*) and noninclusion (*ni*) populations. *B*, Zebra contour plots of AD293 cells transfected with EGFP-tagged proteins and the gates used to define the i and ni populations. The Zebra plot shows each contour as a *shaded* gradient (*white* to *black* from the lowest to highest point) spaced at 5% increments. *C*, enrichment of cells containing inclusions or lacking inclusions after sorting. i and ni populations were imaged by microscopy after sorting and counted for proportions of cells with or without inclusions. Significance was evaluated by *Z*-test (*n* values: 37A, unsorted 370, ni 79, i 77; A4V, unsorted 299, ni 48, i 67; G85R, unsorted 148, ni 64, i 55; 72Q, unsorted 161, ni 56, i 81); *, $p < 0.01$. Cell populations were analyzed by SVA and are plotted in the same way as for Fig. 4 for high speed analysis (*D*), low speed analysis (*E*) and lysates supplemented with 2 M sucrose at low speed analysis (*F*).

sequence was a greater extent of carboxypeptidase Y aggregation into a JUNQ-like inclusion (51). The implications of these mechanisms are that for an IPOD-like inclusion to operate as a coping response, this must come at additional cost on the quality control resources and hence may reflect a last resort mitigation effort to save the cell.

The other notable finding from our work was the lack of intermediate sized aggregates between inclusions and the steady-state oligomers. Whereas many previous studies posit small prefibrillar aggregates as toxic (52, 53), it is possible that these species are generally of very low abundance in the cellular environment or are rapidly sequestered into inclusions when they form. This contrasts to our prior work with Httex1, which indicated a pool of ~17% oligomeric species of ~140 S (10, 12).

It remains plausible that oligomers are incidental to more acute problems of aggregation or that different flanking sequences can modulate rate-limiting steps in an aggregation pathway or interaction with quality control machinery. Other studies have suggested that differences in assembly of poly(Q)-based aggregates is mediated by the flanking regions (10, 54), and others have postulated that chaperones/other proteins involved in inclusion formation can interact at the flanking sequences which may also account for these oligomers (55, 56). It remains possible that quality control processes do not allow the intermediate aggregates to accumulate to great extents in the cytosol by actively removing them or coalescing them into the IPOD and JUNQ structures when the quality control capacity for degradation or disaggregation becomes exceeded. Recent studies
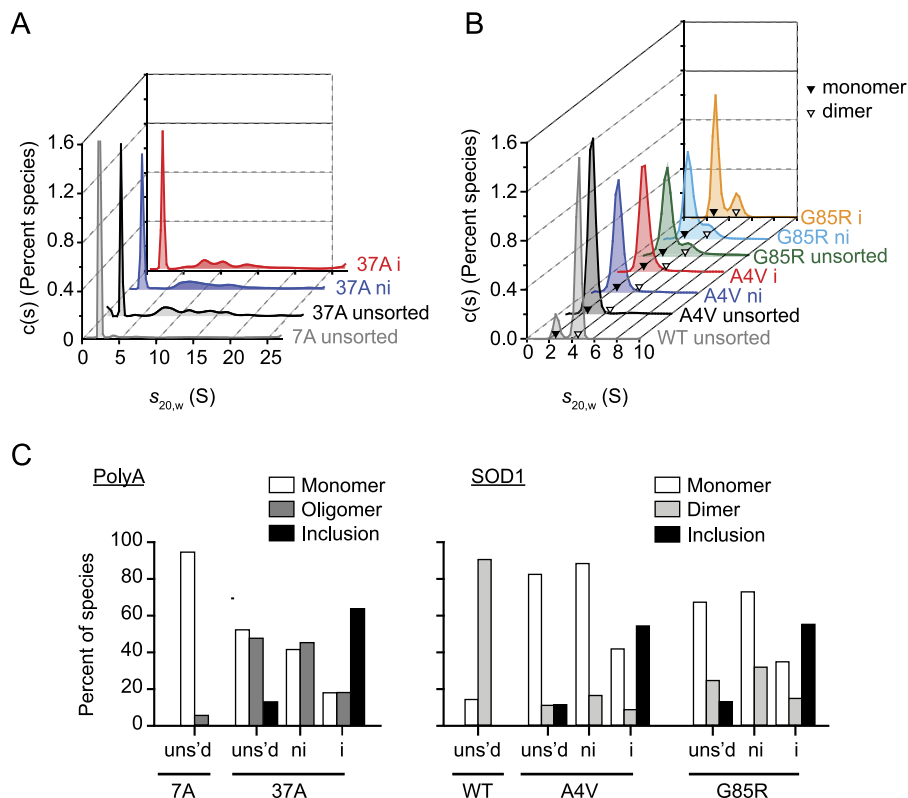
FIGURE 7. **Size distributions and molecular partitioning of EGFP-tagged protein and homopolypeptides in cells with inclusions and those without inclusions.** *A*, $c(s)$ size distribution analysis of poly(A) variants. *B*, $c(s)$ analysis of SOD1 variants, with estimated (homo)oligomeric state indicated. *C*, proportion of molecules in major oligomeric classes, calculated as described in Fig. 5*B* legend using the raw data from Fig. 6.

support a role for quality control mechanisms recognizing soluble poly(Q)-expanded Httex1 forms and degrading them faster than the shorter (25Q) form (57).

Collectively, our study suggests that mutations that lead to protein aggregates in the long term of disease pathologies for JUNQ-forming protein, in fact place the greatest change on proteins at the steady-state level. For SOD1, this would posit the monomer as a source of toxicity and one that is constitutively onerous to cell health. Hence, aggregation is more likely a symptom of late stage collapse of quality control systems rather than the cause of toxicity in the first place.

REFERENCES

1. Sipe, J. D., Benson, M. D., Buxbaum, J. N., Ikeda, S., Merlini, G., Saraiva, M. J., and Westermark, P. (2010) Amyloid fibril protein nomenclature: 2010 recommendations from the nomenclature committee of the International Society of Amyloidosis. *Amyloid* **17,** 101–104
2. Hatters, D. M. (2012) Putting huntingtin "aggregation" in view with windows into the cellular milieu. *Curr. Top. Med. Chem.* **12,** 2611–2622
3. Shorter, J. (2011) The mammalian disaggregase machinery: Hsp110 synergizes with Hsp70 and Hsp40 to catalyze protein disaggregation and reactivation in a cell-free system. *PloS One* **6,** e26319
4. Rampelt, H., Kirstein-Miles, J., Nillegoda, N. B., Chi, K., Scholz, S. R., Morimoto, R. I., and Bukau, B. (2012) Metazoan Hsp70 machines use Hsp110 to power protein disaggregation. *EMBO J.* **31,** 4221–4235
5. Tyedmers, J., Mogk, A., and Bukau, B. (2010) Cellular strategies for controlling protein aggregation. *Nat. Rev. Mol. Cell Biol.* **11,** 777–788
6. Hartl, F. U., Bracher, A., and Hayer-Hartl, M. (2011) Molecular chaperones in protein folding and proteostasis. *Nature* **475,** 324–332
7. Kaganovich, D., Kopito, R., and Frydman, J. (2008) Misfolded proteins partition between two distinct quality control compartments. *Nature* **454,** 1088–1095
8. Johnston, J. A., Ward, C. L., and Kopito, R. R. (1998) Aggresomes: a cellular response to misfolded proteins. *J. Cell Biol.* **143,** 1883–1898
9. Ramdzan, Y. M., Nisbet, R. M., Miller, J., Finkbeiner, S., Hill, A. F., and Hatters, D. M. (2010) Conformation sensors that distinguish monomeric proteins from oligomers in live cells. *Chem. Biol.* **17,** 371–379
10. Olshina, M. A., Angley, L. M., Ramdzan, Y. M., Tang, J., Bailey, M. F., Hill, A. F., and Hatters, D. M. (2010) Tracking mutant huntingtin aggregation kinetics in cells reveals three major populations that include an invariant oligomer pool. *J. Biol. Chem.* **285,** 21807–21816
11. Ramdzan, Y. M., Polling, S., Chia, C. P., Ng, I. H., Ormsby, A. R., Croft, N. P., Purcell, A. W., Bogoyevitch, M. A., Ng, D. C., Gleeson, P. A., and Hatters, D. M. (2012) Tracking protein aggregation and mislocalization in cells with flow cytometry. *Nat. Methods* **9,** 467–470
12. Ormsby, A. R., Ramdzan, Y. M., Mok, Y. F., Jovanoski, K. D., and Hatters, D. M. (2013) A platform to view huntingtin exon 1 aggregation flux in the cell reveals divergent influences from chaperones hsp40 and hsp70. *J. Biol. Chem.* **288,** 37192–37203
13. Lebowitz, J., Lewis, M. S., and Schuck, P. (2002) Modern analytical ultracentrifugation in protein science: a tutorial review. *Protein Sci.* **11,** 2067–2079
14. Irtegun, S., Wood, R. J., Ormsby, A. R., Mulhern, T. D., and Hatters, D. M. (2013) Tyrosine 416 is phosphorylated in the closed, repressed conformation of c-Src. *PLoS One* **8,** e71035
15. Matsumoto, G., Kim, S., and Morimoto, R. I. (2006) Huntingtin and mutant SOD1 form aggregate structures with distinct molecular properties in human cells. *J. Biol. Chem.* **281,** 4477–4485

16. Weisberg, S. J., Lyakhovetsky, R., Werdiger, A. C., Gitler, A. D., Soen, Y., and Kaganovich, D. (2012) Compartmentalization of superoxide dismutase 1 (SOD1G93A) aggregates determines their toxicity. *Proc. Natl. Acad. Sci. U.S.A.* **109,** 15811–15816

17. Berger, Z., Davies, J. E., Luo, S., Pasco, M. Y., Majoul, I., O'Kane, C. J., and Rubinsztein, D. C. (2006) Deleterious and protective properties of an aggregate-prone protein with a polyalanine expansion. *Hum. Mol. Genet.* **15,** 453–465

18. Zoghbi, H. Y., and Orr, H. T. (2000) Glutamine repeats and neurodegeneration. *Annu. Rev. Neurosci.* **23,** 217–247

19. Onodera, O., Burke, J. R., Miller, S. E., Hester, S., Tsuji, S., Roses, A. D., and Strittmatter, W. J. (1997) Oligomerization of expanded-polyglutamine domain fluorescent fusion proteins in cultured mammalian cells. *Biochem. Biophys. Res. Commun.* **238,** 599–605

20. Marsh, J. L., Walker, H., Theisen, H., Zhu, Y. Z., Fielder, T., Purcell, J., and Thompson, L. M. (2000) Expanded polyglutamine peptides alone are intrinsically cytotoxic and cause neurodegeneration in *Drosophila. Hum. Mol. Genet.* **9,** 13–25

21. Hughes, J., and Thomas, P. (2013) in *Tandem Repeats in Genes, Proteins, and Disease* (Hatters, D. M., and Hannan, A. J., eds) pp. 135–151, Humana Press, Totowa, NJ

22. Rankin, J., Wyttenbach, A., and Rubinsztein, D. C. (2000) Intracellular green fluorescent protein-polyalanine aggregates are associated with cell death. *Biochem. J.* **348,** 15–19

23. Nojima, J., Oma, Y., Futai, E., Sasagawa, N., Kuroda, R., Turk, B., and Ishiura, S. (2009) Biochemical analysis of oligomerization of expanded polyalanine repeat proteins. *J. Neurosci. Res.* **87,** 2290–2296

24. Bruijn, L. I., Houseweart, M. K., Kato, S., Anderson, K. L., Anderson, S. D., Ohama, E., Reaume, A. G., Scott, R. W., and Cleveland, D. W. (1998) Aggregation and motor neuron toxicity of an ALS-linked SOD1 mutant independent from wild-type SOD1. *Science* **281,** 1851–1854

25. Turner, B. J., Atkin, J. D., Farg, M. A., Zang, D. W., Rembach, A., Lopes, E. C., Patch, J. D., Hill, A. F., and Cheema, S. S. (2005) Impaired extracellular secretion of mutant superoxide dismutase 1 associates with neurotoxicity in familial amyotrophic lateral sclerosis. *J. Neurosci.* **25,** 108–117

26. Kabeya, Y., Mizushima, N., Ueno, T., Yamamoto, A., Kirisako, T., Noda, T., Kominami, E., Ohsumi, Y., and Yoshimori, T. (2000) LC3, a mammalian homologue of yeast Apg8p, is localized in autophagosome membranes after processing. *EMBO J.* **19,** 5720–5728

27. Lide, D. R. (ed) (1996) *CRC Handbook of Chemistry and Physics*, CRC Press, Boca Raton, FL

28. Schuck, P., Perugini, M. A., Gonzales, N. R., Howlett, G. J., and Schubert, D. (2002) Size-distribution analysis of proteins by analytical ultracentrifugation: strategies and application to model systems. *Biophys. J.* **82,** 1096–1111

29. Deng, H. X., Hentati, A., Tainer, J. A., Iqbal, Z., Cayabyab, A., Hung, W. Y., Getzoff, E. D., Hu, P., Herzfeldt, B., and Roos, R. P. (1993) Amyotrophic lateral sclerosis and structural defects in Cu,Zn superoxide dismutase. *Science* **261,** 1047–1051

30. Rosen, D. R., Siddique, T., Patterson, D., Figlewicz, D. A., Sapp, P., Hentati, A., Donaldson, D., Goto, J., O'Regan, J. P., Deng, H. X., Rahmani, Z., Krizus, A., McKenna-Yasek, D., Cayabyab, A., Gaston, S. M., Berger, R., Tanzi, R. E., Halperin, J. J., Herzfeldt, B., Van den Bergh, R., Hung, W. Y., Bird, T., Deng, G., Mulder, D. W., Smyth, C., Laing, N. G., Soriano, E., Pericak-Vance, M. A., Haines, J., Rouleau, G. A., Gusella, J. S., Horvitz, H. R., and Brown, R. H. (1993) Mutations in Cu/Zn superoxide dismutase gene are associated with familial amyotrophic lateral sclerosis. *Nature* **362,** 59–62

31. Kim, S., Nollen, E. A., Kitagawa, K., Bindokas, V. P., and Morimoto, R. I. (2002) Polyglutamine protein aggregates are dynamic. *Nat. Cell Biol.* **4,** 826–831

32. Arrasate, M., Mitra, S., Schweitzer, E. S., Segal, M. R., and Finkbeiner, S. (2004) Inclusion body formation reduces levels of mutant huntingtin and the risk of neuronal death. *Nature* **431,** 805–810

33. Schuck, P. (2000) Size-distribution analysis of macromolecules by sedimentation velocity ultracentrifugation and lamm equation modeling. *Biophys. J.* **78,** 1606–1619

34. Tycko, R. (2011) Solid-state NMR studies of amyloid fibril structure. *Annu. Rev. Phys. Chem.* **62,** 279–299

35. Bernacki, J. P., and Murphy, R. M. (2011) Length-dependent aggregation of uninterrupted polyalanine peptides. *Biochemistry* **50,** 9200–9211

36. Lindberg, M. J., Byström, R., Boknäs, N., Andersen, P. M., and Oliveberg, M. (2005) Systematically perturbed folding patterns of amyotrophic lateral sclerosis (ALS)-associated SOD1 mutants. *Proc. Natl. Acad. Sci. U.S.A.* **102,** 9754–9759

37. Matsumoto, G., Stojanovic, A., Holmberg, C. I., Kim, S., and Morimoto, R. I. (2005) Structural properties and neuronal toxicity of amyotrophic lateral sclerosis-associated Cu/Zn superoxide dismutase 1 aggregates. *J. Cell Biol.* **171,** 75–85

38. Karch, C. M., Prudencio, M., Winkler, D. D., Hart, P. J., and Borchelt, D. R. (2009) Role of mutant SOD1 disulfide oxidation and aggregation in the pathogenesis of familial ALS. *Proc. Natl. Acad. Sci. U.S.A.* **106,** 7774–7779

39. Banci, L., Bertini, I., Durazo, A., Girotto, S., Gralla, E. B., Martinelli, M., Valentine, J. S., Vieru, M., and Whitelegge, J. P. (2007) Metal-free superoxide dismutase forms soluble oligomers under physiological conditions: a possible general mechanism for familial ALS. *Proc. Natl. Acad. Sci. U.S.A.* **104,** 11263–11267

40. Münch, C., and Bertolotti, A. (2010) Exposure of hydrophobic surfaces initiates aggregation of diverse ALS-causing superoxide dismutase-1 mutants. *J. Mol. Biol.* **399,** 512–525

41. Blondelle, S. E., Forood, B., Houghten, R. A., and Pérez-Payá, E. (1997) Polyalanine-based peptides as models for self-associated β-pleated-sheet complexes. *Biochemistry* **36,** 8393–8400

42. Bennett, M. J., Huey-Tubman, K. E., Herr, A. B., West, A. P., Jr., Ross, S. A., and Bjorkman, P. J. (2002) A linear lattice model for polyglutamine in CAG-expansion diseases. *Proc. Natl. Acad. Sci. U.S.A.* **99,** 11634–11639

43. Chen, S., Ferrone, F. A., and Wetzel, R. (2002) Huntington's disease age-of-onset linked to polyglutamine aggregation nucleation. *Proc. Natl. Acad. Sci. U.S.A.* **99,** 11884–11889

44. Cohen, S. I., Vendruscolo, M., Dobson, C. M., and Knowles, T. P. (2012) From macroscopic measurements to microscopic mechanisms of protein aggregation. *J. Mol. Biol.* **421,** 160–171

45. Perutz, M. F., Johnson, T., Suzuki, M., and Finch, J. T. (1994) Glutamine repeats as polar zippers: their possible role in inherited neurodegenerative diseases. *Proc. Natl. Acad. Sci. U.S.A.* **91,** 5355–5358

46. Scherzinger, E., Sittler, A., Schweiger, K., Heiser, V., Lurz, R., Hasenbank, R., Bates, G. P., Lehrach, H., and Wanker, E. E. (1999) Self-assembly of polyglutamine-containing huntingtin fragments into amyloid-like fibrils: implications for Huntington's disease pathology. *Proc. Natl. Acad. Sci. U.S.A.* **96,** 4604–4609

47. Chen, S., Berthelier, V., Hamilton, J. B., O'Nuallain, B., and Wetzel, R. (2002) Amyloid-like features of polyglutamine aggregates and their assembly kinetics. *Biochemistry* **41,** 7391–7399

48. Wang, J., Farr, G. W., Zeiss, C. J., Rodriguez-Gil, D. J., Wilson, J. H., Furtak, K., Rutkowski, D. T., Kaufman, R. J., Ruse, C. I., Yates, J. R., 3rd, Perrin, S., Feany, M. B., and Horwich, A. L. (2009) Progressive aggregation despite chaperone associations of a mutant SOD1-YFP in transgenic mice that develop ALS. *Proc. Natl. Acad. Sci. U.S.A.* **106,** 1392–1397

49. Wang, M., Weiss, M., Simonovic, M., Haertinger, G., Schrimpf, S. P., Hengartner, M. O., and von Mering, C. (2012) PaxDb, a database of protein abundance averages across all three domains of life. *Mol. Cell. Proteomics* **11,** 492–500

50. Gidalevitz, T., Ben-Zvi, A., Ho, K. H., Brignull, H. R., and Morimoto, R. I. (2006) Progressive disruption of cellular protein folding in models of polyglutamine diseases. *Science* **311,** 1471–1474

51. Park, S. H., Kukushkin, Y., Gupta, R., Chen, T., Konagai, A., Hipp, M. S., Hayer-Hartl, M., and Hartl, F. U. (2013) Poly(Q) proteins interfere with nuclear degradation of cytosolic proteins by sequestering the Sis1p chaperone. *Cell* **154,** 134–145

52. Lotz, G. P., and Legleiter, J. (2013) The role of amyloidogenic protein oligomerization in neurodegenerative disease. *J. Mol. Med.* **91,** 653–664

53. Cecchi, C., and Stefani, M. (2013) The amyloid-cell membrane system: the interplay between the biophysical features of oligomers/fibrils and cell membrane defines amyloid toxicity. *Biophys. Chem.* **182,** 30–43

54. Robertson, A. L., and Bottomley, S. P. (2010) Towards the treatment of polyglutamine diseases: the modulatory role of protein context. *Curr. Med. Chem.* **17,** 3058–3068

55. Wang, Y., Meriin, A. B., Zaarur, N., Romanova, N. V., Chernoff, Y. O., Costello, C. E., and Sherman, M. Y. (2009) Abnormal proteins can form aggresome in yeast: aggresome-targeting signals and components of the machinery. *FASEB J.* **23,** 451–463

56. Robertson, A. L., Headey, S. J., Saunders, H. M., Ecroyd, H., Scanlon, M. J., Carver, J. A., and Bottomley, S. P. (2010) Small heat-shock proteins inter-act with a flanking domain to suppress polyglutamine aggregation. *Proc. Natl. Acad. Sci. U.S.A.* **107,** 10424–10429

57. Tsvetkov, A. S., Arrasate, M., Barmada, S., Ando, D. M., Sharma, P., Shaby, B. A., and Finkbeiner, S. (2013) Proteostasis of polyglutamine varies among neurons and predicts neurodegeneration. *Nat. Chem. Biol.* **9,** 586–592